Late Eocene evolution of the Çiçekdağı Basin (central Turkey): Syn-sedimentary compression during microcontinent–continent collision in central Anatolia

Erhan Gülyüz [a], Nuretdin Kaymakci [a,b], Maud J.M. Meijers [c], Douwe J.J. van Hinsbergen [d,e,*], Côme Lefebvre [c,f], Reinoud L.M. Vissers [f], Bart W.H. Hendriks [g], A. Ahmet Peynircioğlu [b]

[a] Middle East Technical University, Department of Geological Engineering, 06531 Ankara, Turkey
[b] Paleomagnetic Laboratory "Fort Hoofddijk", Faculty of Geosciences, Utrecht University, Budapestlaan 17, 3584 CD Utrecht, The Netherlands
[c] Observatoire de la Côte d'Azur, Université de Nice Sophia Antipolis Géoazur, Parc Valrose, 06108 Nice cedex 2, France
[d] Physics of Geological Processes, University of Oslo, SemSælandsvei 6, 0316 Oslo, Norway
[e] Center for Advanced Study, Norwegian Academy of Science and Letters, Drammensveien 78, 0271 Oslo, Norway
[f] Structural Geology and Tectonics Group, Faculty of Geosciences, Utrecht University, Budapestlaan 4, 3584 CD Utrecht, the Netherlands
[g] Center for Geodynamics, Geological Survey of Norway (NGU), Leiv Eirikssons vei 39, 7491 Trondheim, Norway

ARTICLE INFO

ABSTRACT

The Central Anatolian Crystalline Complex (CACC) exposes metasediment rocks overlain by Cretaceous ophiolites and intruded by granitoids. Following late Cretaceous exhumation of its high-grade metamorphic rocks, the CACC started to collide with the Central Pontides of southern Eurasia in the latest Cretaceous to Paleocene. Here, we present the sedimentary, stratigraphic and tectonic evolution of the Çiçekdağı Basin, located in the northwest of the CACC. Magnetostratigraphic dating, supported by $^{40}Ar/^{39}Ar$ geochronology, shows a late Eocene basin age. The basin fill unconformably overlies metamorphic basement in the south and ophiolites of the CACC in the north. It consists of red conglomerates, sandstones and siltstones, which overlie a sequence of nummulitic limestones. In the south, these limestones are ~10 m thick, are underlain by a few meters of conglomerate unit unconformably covering the CACC metamorphics. In the north, the limestones are underlain by a ~200 m thick sequence of volcanics and fine-grained clastics intercalating with shallow marine black shales. The upper Eocene sediments of the Çiçekdağı Basin were deformed into a syn-anticline pair. Progressive unconformities in the northern flank and a rapid and persistent ~180° switch in paleocurrent directions from southward to northward in the southern flank of the anticline demonstrate syn-sedimentary folding. We interpret the folding to result from a southward progression of the Çankırı foreland basin as a result of ongoing collision between the CACC and the Pontides.

1. Introduction

The Alpine belt of the (circum-) Mediterranean region is marked by a series of continental domains in which extension has led to the exhumation of high-grade metamorphic rocks. These extensional domains are commonly interpreted as extensionally thinned overriding plates exposing rocks that were metamorphosed in and above subduction zones (Bozkurt and Oberhänsli, 2001; Jolivet et al., 2009; Vissers et al., 1995). The Central Anatolian Crystalline Complex (CACC, also known as the Kırşehir Block) in central Turkey is one of the largest metamorphic terranes in the Alpine orogen now preserved in a 250×250× 250 km triangular region (Göncüoğlu et al., 1991; Şengör and Yılmaz, 1981) (Fig. 1). It developed in a context of closure of the Neotethyan Ocean and exposes (a) high-grade metamorphic rocks (the Central Anatolian Metamorphics, CAM) with Cretaceous metamorphic ages,

underlying (b) Cretaceous supra-subduction-type ophiolites (Central Anatolian Ophiolites, CAO), both intruded and overlain by (c) felsic and mafic magmatic rocks (Erkan, 1976; Seymen, 1981; Whitney et al., 2001; Yalınız et al., 2000a,b).

The CACC is separated from the Sakarya continental block of the Pontides towards the north, which belonged to Eurasia since at least Jurassic times (Meijers et al., 2010b; Torsvik and Cocks, 2009), by the İzmir–Ankara–Erzincan suture zone (Okay, 2008). This suture zone is marked by a mélange, which includes ocean-floor pillow basalts, commonly with MORB geochemical signatures, and deep-marine sediments of Triassic–Cretaceous age offscraped from an oceanic plate that subducted below the Pontides before the CACC–Pontide collision (Dilek and Thy, 2006; Gökten and Floyd, 2007; Tekin et al., 2002; Tüysüz et al., 1995). The CACC is overlain by ophiolites with Turonian–Santonian epi-ophiolitic cover sediments, and with a supra-subduction zone geochemical signature (Yalınız et al., 2000b). Fringing the CACC to the south, a belt of upper Cretaceous high-pressure metamorphic rocks separates the CACC from the non-metamorphosed Tauride fold-thrust belt (Fig. 1) marking the location of a late Cretaceous subduction zone

* Corresponding author at: Physics of Geological Processes, University of Oslo, SemSælandsvei 6, 0316 Oslo, Norway.
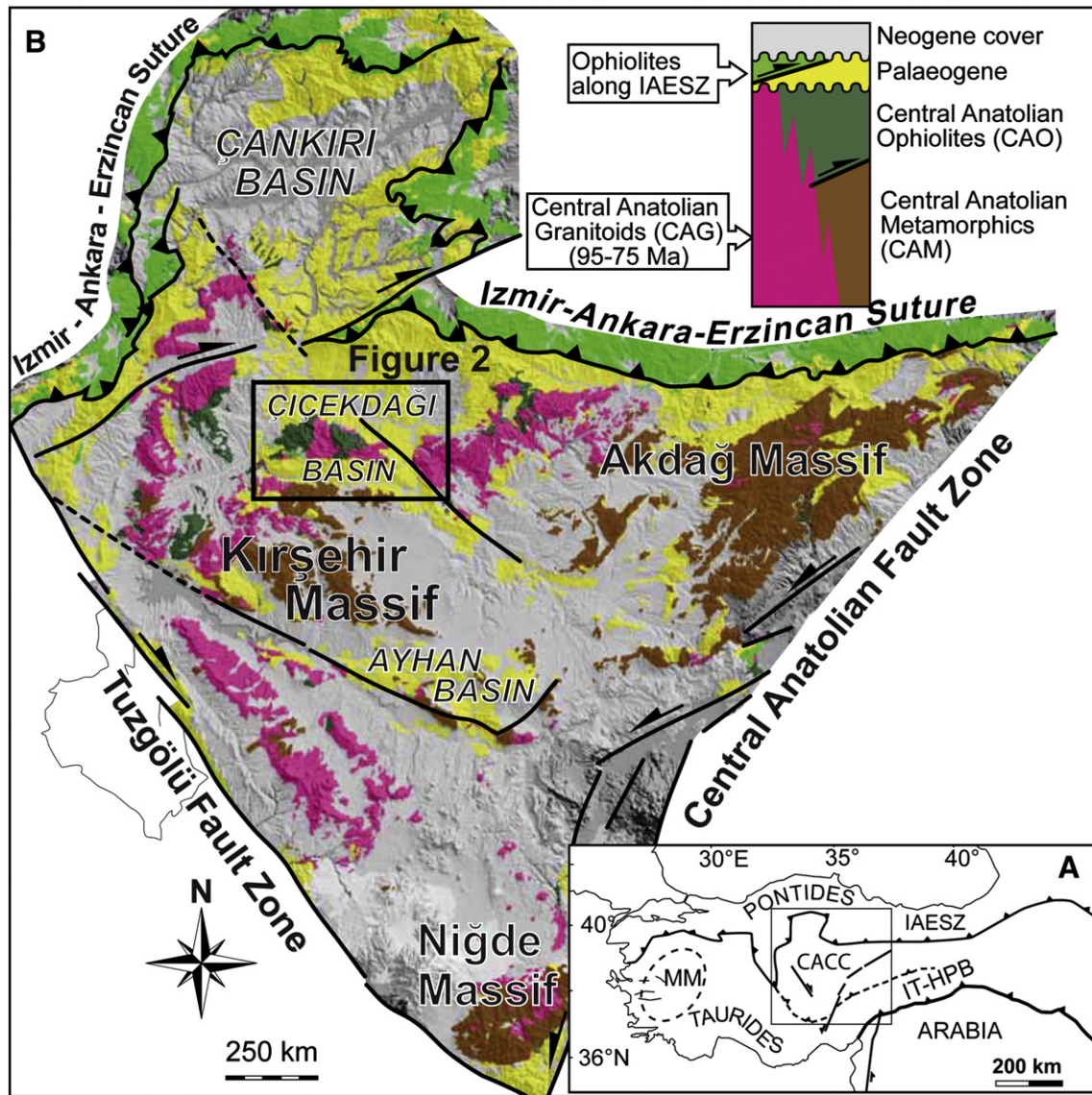E-mail address: d.v.hinsbergen@fys.uio.no (D.J.J. van Hinsbergen).

Fig. 1. (A) Location of the Menderes Massif (MM), the CACC, İzmir–Ankara–Erzincan Suture Zone, (IAESZ), and the Intra–Tauride High Pressure Belt (IT-HPB) in the Turkish orogenic system. (B) Simplified geological map of the CACC draped on a Digital Elevation Model. The black rectangle indicates the study area. Top right: simplified tectono-stratigraphic column showing the relationship between the main units of the CACC (not in scale).
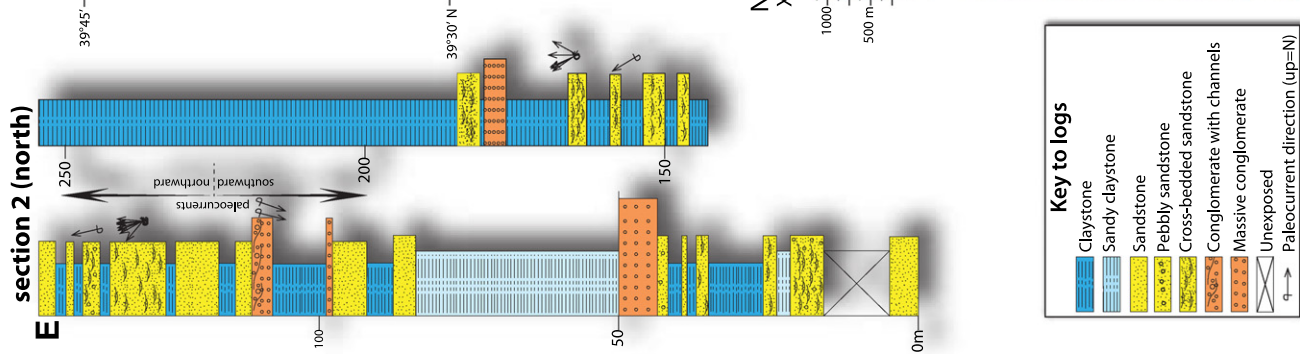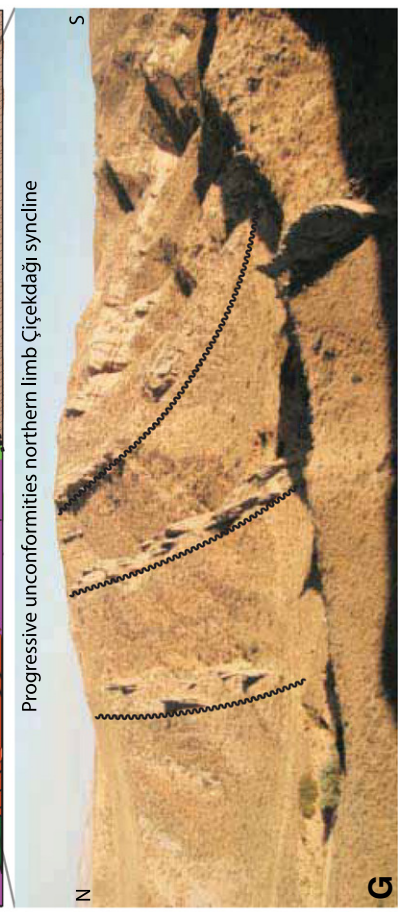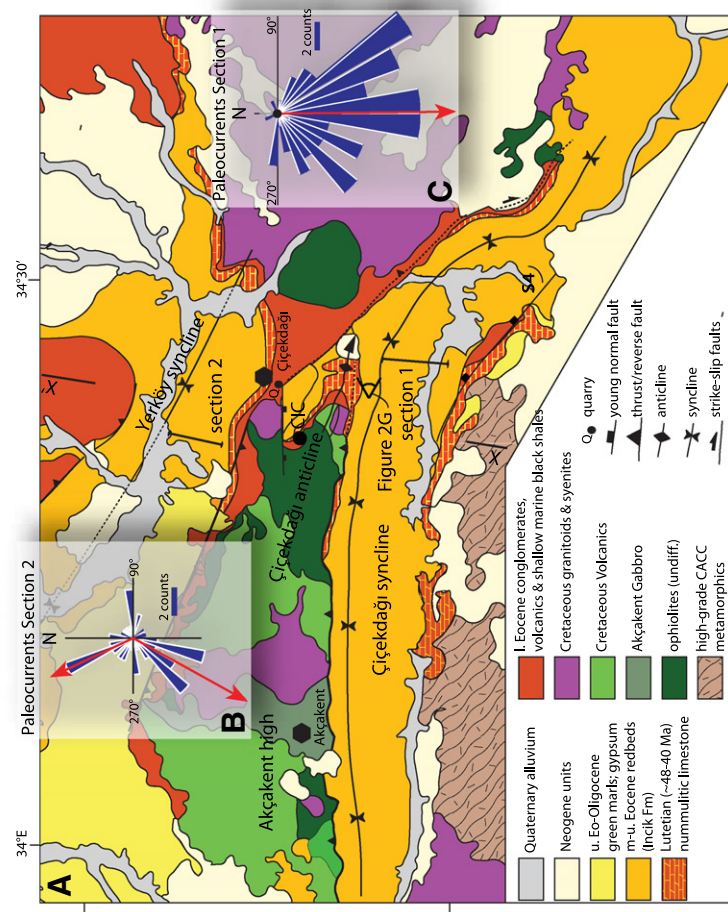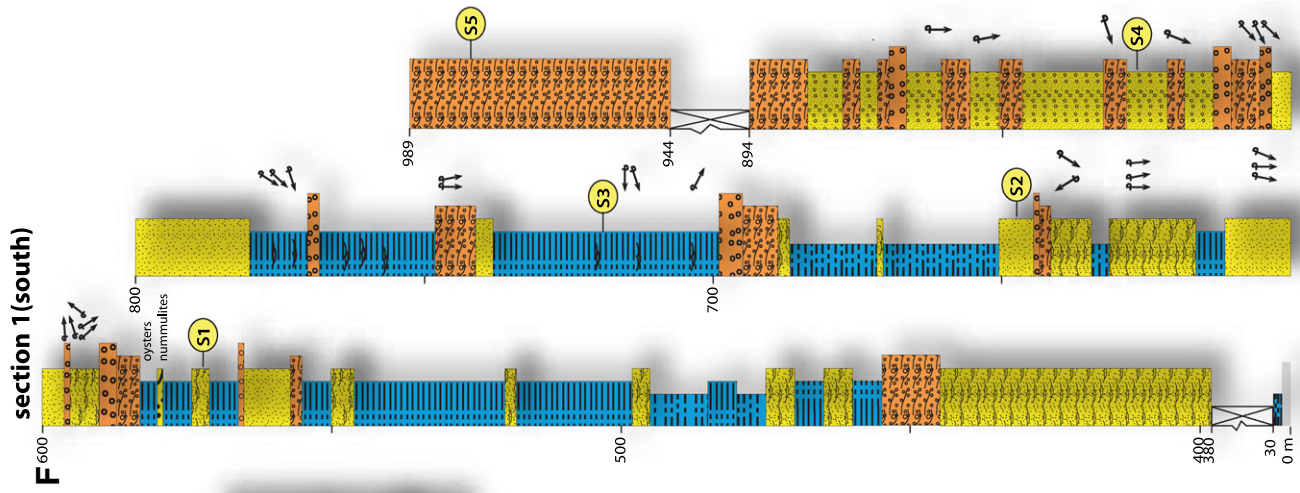
(Okay, 1984, 1986; Pourteau et al., 2010). The Taurides and the CACC were derived from a continental fragment, or fragments, that rifted away from Gondwana, probably in the Triassic (Frizon de Lamotte et al., 2011; Okay et al., 1996; Şengör and Yılmaz, 1981).

The geological history of the CACC can roughly be subdivided into three major tectonic episodes. (1) Ophiolite emplacement: in late Cretaceous times (~95 Ma), platform carbonates and continental clastics, underthrusted an oceanic overriding plate (Boztuğ et al., 2007; Floyd et al., 2000; Yalınız et al., 2000a,b,c). This was followed by high-temperature metamorphism at low to intermediate pressures and intrusion of widespread plutons (Boztuğ et al., 2007, 2009b; Kadıoğlu et al., 2003; Whitney and Hamilton, 2004; Whitney et al., 2001). (2) Exhumation: thermochronological data show that CACC rocks exhumed in late Cretaceous to Paleogene times (Boztuğ and Jonckheere, 2007; Boztuğ et al., 2009a; Gautier et al., 2002), and in a few places, discrete extensional shear zones within the granitoids (Isık, 2009; Isık et al., 2008), and extensional detachments exhuming metamorphic rocks (Gautier et al., 2008; Lefebvre et al., 2011, submitted for publication) have been demonstrated. (3) Collision with

the Pontides: exhumation of the CACC was followed by renewed contraction (Boztuğ et al., 2009b; Clark and Robertson, 2005; Dirik et al., 1999; Göncüoğlu et al., 1991; Yılmaz and Yılmaz, 2006) related to Paleogene collision of the CACC with the Pontides (Kaymakcı et al., 2000, 2003a,b, 2009; Meijers et al., 2010a; Rice et al., 2006). Recently, Genç and Yurur (2010) argued that extension and exhumation of the CACC were contemporaneous with compression around the margins of the CACC. These authors argued that all compression related to gravitational collapse of the CACC. We will come back to this issue in the discussion.

Since late Miocene time, the present-day boundaries of the CACC were formed by strike-slip faults (Aydemir and Ateş, 2006; Kaymakcı et al., 2010; Koçyiğit and Beyhan, 1998), probably related to westward Anatolian extrusion away from Arabia (Şengör et al., 1985).

The CACC is in places covered and surrounded by folded and thrusted Paleogene sediments and volcanics (e.g., Göncüoğlu et al., 1993; Seymen, 1981; Yürür and Genç, 2006). The late Cretaceous to Miocene Çankırı sedimentary basin to the north of the CACC (Fig. 1) has been used to constrain the Paleogene collision history of the CACC with the Pontides,

section 1 (south)

section 2 (north)

Key to logs

Claystone
Sandy claystone
Sandstone
Pebbly sandstone
Cross-bedded sandstone
Conglomerate with channels
Massive conglomerate
Unexposed
Paleocurrent direction (up=N)

Paleocurrents Section 1

Paleocurrents Section 2

Quaternary alluvium
Neogene units
u. Eo-Oligocene
green marls; gypsum
m–u. Eocene redbeds (Incik Fm)
Lutetian (~48–40 Ma) nummulitic limestone
l. Eocene conglomerates, volcanics & shallow marine black shales
Cretaceous granitoids & syenites
Cretaceous Volcanics
Akçakent Gabbro
ophiolites (undiff.)
high-grade CACC metamorphics

quarry
young normal fault
thrust/reverse fault
anticline
syncline
strike-slip faults

Çiçekdağı anticline
Çiçekdağı syncline
Yerköy syncline
section 2
section 1
Figure 2G
Akçakent high

Progressive unconformities northern limb Çiçekdağı syncline

paleocurrents
southward northward

because the Paleogene part of its infill straddles the İzmir–Ankara suture. For clarity: we define the 'collision history' as the period between the first contact between the CACC and the Pontides, and the end of contraction between these two units. Kaymakcı et al. (2009) identified two main tectonic stages of this basin: its upper Cretaceous stratigraphy does not straddle the suture, and is restricted to the part of the basin overlying the Pontides and suture zone rocks. These authors interpreted the late Cretaceous history as a forearc basin above a northward dipping subduction zone. The Paleocene and younger sediments display foreland basin characteristics, and do straddle the suture. Sediments of similar lithostratigraphy to the Paleogene Çankırı Basin are found as far south as the present-day Çiçekdağı syncline (Fig. 2). Sedimentary rocks in the southern flank of this syncline unconformably cover high-grade metamorphic rocks of the CACC. In the core of the Çiçekdağı anticline immediately north of the Çiçekdağı syncline, layered and isotropic gabbro, plagiogranite, dolerite dyke complexes, basaltic lavas and epi-ophiolitic sediments, intruded by late Cretaceous felsic plutons are exposed (Fig. 2) (Yalınız et al., 2000a), as well as marble lenses. We studied the sedimentary, stratigraphic and structural evolution of the Çiçekdağı region, and provide magnetostratigraphy combined with ^{40}Ar/^{39}Ar geochronology to date the basin fill. We depict the sediments exposed on the southern side of the Çiçekdağı anticline as the 'Çiçekdağı Basin' in this paper, although we will show that during the early stages of basin fill, this basin can be viewed as the southward propagation of the Çankırı Basin. We aim to determine the relationship between Eocene sedimentation and contractional tectonics in the NW part of the CACC and we will discuss our results in the context of the timing of exhumation of the CACC relative to its collision with the Pontides.

2. Geology of the Çiçekdağı anticline and syncline

The Çiçekdağı region exposes deformed Cenozoic shallow marine and continental sedimentary rocks and lavas, overlying pre-Cenozoic basement. To the south, this basement comprises high-grade metasediments of the CACC. Within the core of the Akçakent high, the basement consists of mid-upper Cretaceous ophiolites of the CAO, intruded by Cretaceous monzogranites and syenites (Ketin, 1955; Yalınız et al., 2000a; Yılmaz and Boztuğ, 1998), as well as some isolated marble lenses that may belong to the high-grade metasediments of the CACC.

2.1. Basement units

The Çiçekdağı Basin is bounded in the south by metasedimentary rocks of the CACC, which form the northernmost exposures of the CAM, and by the Çiçekdağı Ophiolite (of the CAO) in the north. The CAM rocks along the southern margin of the basin consist of marbles, calcsilicates and pelitic schists. Their general structure shows a well-developed and consistent foliation dipping in a N or NW direction, subparallel, or at a small angle to the orientation of the unconformably overlying sediments in the southern limb of the Çiçekdağı syncline. The dominant minerals in the pelitic compositions comprise quartz and biotite, creating a ribboned texture in the rocks. Also, the association of large potassic feldspar and enclosing fibrous sillimanite points to the dehydration reaction muscovite + quartz = K-feldspar + sillimanite + H$_2$O. The mineral assemblages clearly correspond to high-temperature, amphibolite facies metamorphic conditions, which are also in good agreement with previous estimates on these rocks described in the literature (Erkan, 1976).

To the north of the basin, the Çiçekdağ Ophiolite presents typical features of an ophiolitic crustal sequence with gabbro, plagiogranite, a sheeted dolerite complex and basaltic pillows below the epi-ophiolitic sedimentary cover (note that no ultramafics have been reported) (Yalınız et al., 2000a). The mafic rocks include the Akçakent gabbro and the Çökelik volcanics (Erdoğan et al., 1996). The Akçakent high is cross-cut by a ~N–S trending fault separating the Akçakent gabbro in the east and the Çökelik volcanics in the west (Yılmaz and Boztuğ, 1998). This fault does not crosscut, and therefore predates the Çiçekdağı Basin. The ophiolitic rocks often show greenish colors, which is typically a result of alteration processes. Under the microscope, we identified intensive replacement of the primary magmatic mineral phases (mainly clinopyroxene, plagioclase and oxides) by secondary low-temperature minerals (as actinolite, tremolite, epidote, albite and chlorite). This transformation may result from hydrothermal activity, which usually takes place at the ocean floor just after oceanic crust crystallization as also suggested by Yılmaz and Boztuğ (1998) and Yalınız et al. (2000a). The ophiolite is hence of much lower metamorphic grade than the CAM rocks along the southern margin of the basin.

2.2. General lithostratigraphy of the Çiçekdağı Basin, and regional correlation

The most prominent part of the Çiçekdağı Basin's stratigraphy consists of continental red sandstones and conglomerates. In the south, these conformably overlie ~20 m of fossil-rich nummulitic limestones, which are separated from the high-grade CAM rocks of the CACC by coarse conglomerates, reworking and unconformably covering CAM basement. Nummulitic limestones also conformably underlie red beds on the flanks of Çiçekdağı anticline, but the sedimentary sequence below the limestones here is considerably thicker (at least ~200 m) and consists, from the deepest exposed parts to the top, of shallow marine fossiliferous lignite deposits, overlain by a series of lavas and volcanoclastic deposits. The red bed sequence overlying the nummulitic limestones has a variable thickness of 200–1000 m (see below). We collected a sample (C1) from lavas between black shales and nummulitic limestones in the Çiçekdağı anticline for ^{40}Ar/^{39}Ar dating.

A sequence of nummulitic limestones overlain by red beds is well documented in the Çankırı Basin, where the limestones (Kocaçay Formation) were dated as Lutetian (Kaymakcı et al., 2009), with a numerical age of 48.6–40.4 Ma (Luterbacher et al., 2004). Regionally, red beds overlying the Kocaçay Formation are grouped in the İncik Formation, and palynologically assigned a middle to late Eocene age (Akgün et al., 2002). We collected samples from a long section covering the entire exposed stratigraphy in the southern flank of the Çiçekdağı anticline for a paleomagnetic study addressing the magnetostratigraphy, and to test whether the paleocurrent directions and compression directions associated with folding needed to be corrected for vertical axis rotations.

2.3. Structure and sedimentology of the Çiçekdağı Basin

We subdivide the study area into southern and northern parts, separated by the Akçakent high, which in the eastern part is represented by an anticline (Fig. 2A,D). The syncline to the south hosts the Çiçekdağı Basin is strongly asymmetric and south vergent. A continuous stratigraphy is exposed in ~10° northward-dipping southern limb. At the base of the stratigraphy along the southern flank, nummulitic limestones overlie a several meters thick basal conglomerate section, which unconformably

Fig. 2. (A) Geological map of the Çiçekdağı syncline and anticline, modified from Ketin (1955); (B) Paleocurrent directions of upper Eocene sediments along the northern flank of the Çiçekdağı anticline. The northward paleocurrent directions are younger than the southward directions; see panel (E); (C) Paleocurrent directions of the southern flank of upper Eocene sediments in the Çiçekdağı syncline; (D) Structural cross-section through the Çiçekdağı anticline and syncline; (E) Sedimentary log of upper Eocene sediments in the northern flank of the Çiçekdağı anticline; (F) Sedimentary log of the southern flank of upper Eocene sediments in the Çiçekdağı syncline; (G) Photograph showing progressive unconformities in the northern flank of the Çiçekdağı syncline.
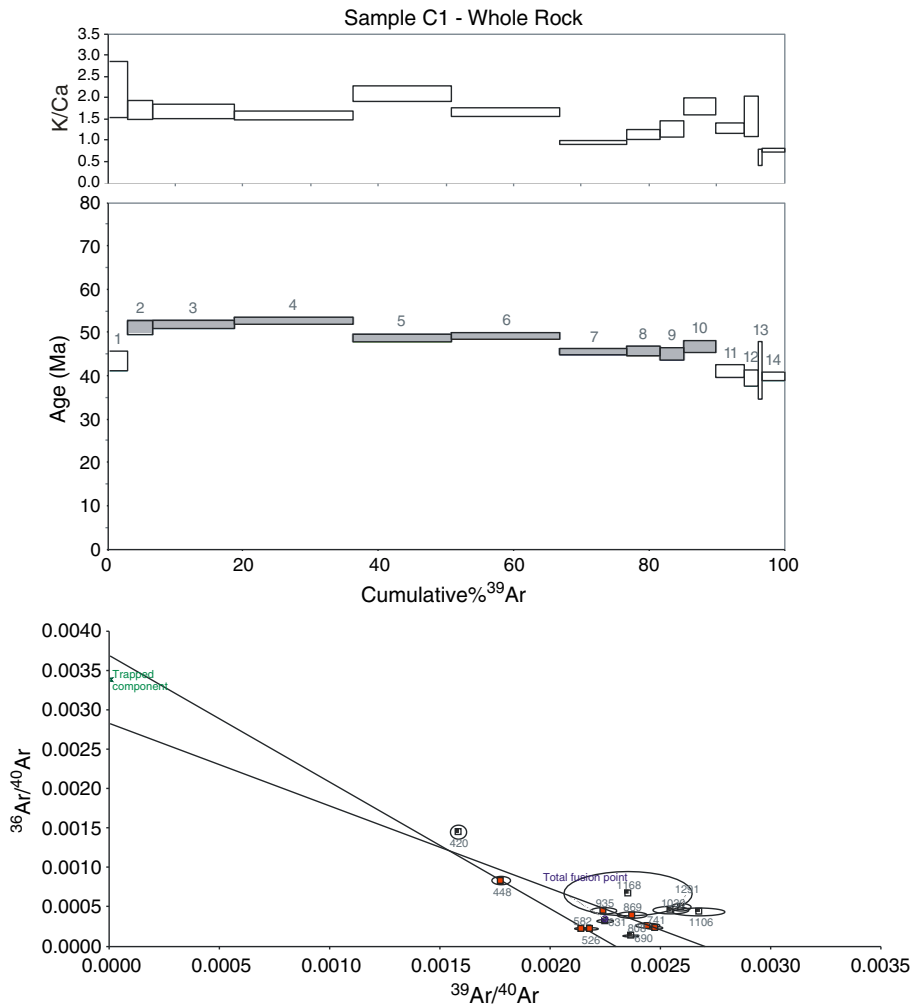
Fig. 3. Step heating release spectra for the samples from sample C1 in the Akçakent high. Each age bar is plotted at the 95% confidence level. The numbers above the age bars correspond to the row number in Appendix 1. Bottom panel shows the inverse isochron diagram.

covers and reworks the high-grade metamorphic rocks of the CACC. The nummulitic limestones become silty towards the top indicating increased influx of continental clastics, but remain shallow marine as shown by giant (up to 30 cm) gastropods within the silty unit. The shallow marine silty limestones grade upward into siltstones and thin (several cm thick) fluvial sandstone lenses with an exposed thickness of ~20 m. We therefore conclude that the transition from shallow marine nummulitic limestones to the continental red clastic series with a total thickness of ~1000 m, is conformable. The lower ~350 m of the red bed stratigraphy is poorly exposed. Above this poorly exposed interval, a continuous section of ~650 m of fluvial red beds is exposed. The bedding orientation on either side of the non-exposed interval is parallel and we have no reason to infer a structural discontinuity in the non-exposed interval.

Section 1 exposes a coarsening upward sequence of stacked lenticular sandstone and conglomerate bodies, with frequent cross-bedding. Around 600 m above the base of the stratigraphy, a several meter thick interval was encountered in the river gully where we measured our section, with foresets draped by thin clay layers suggesting tidal influence, containing in situ oysters and nummulites, suggesting that the first half of the stratigraphy was deposited in environments close enough to sea level to allow for an occasional marine incursion. Although sporadic fragments occur of high-grade schists of the CAM, detrital clasts are dominated by mafic rocks derived from ophiolites and/or the Ankara mélange, and by widespread nummulitic limestones in the upper half of the stratigraphy indicating that during

sedimentation of the Çiçekdağı red beds, units conformably underlying these red beds became reworked.

In order to explore the nature of the source area that provided the clastic detritus in the basin, five samples (S1–S5, indicated in Fig. 2F) of mostly fine-grained sandstones from section 1 have been investigated in light microscopy. The sediment petrography reveals a notable difference between sample S1 and the other, stratigraphically higher samples, consistent with our observations on coarser clastic material from the base of the section as mentioned above. Sample S1 contains clearly metamorphic detritus including grains of glaucophane and garnet absent in the other four samples, while it has a very low content of potassic feldspar and therefore does not seem to contain much detritus from felsic plutonic origin. In addition, sample S1 contains detrital grains of fine-grained phyllite, and notably less bioclastic material than all of the other samples.

Samples S2–S5 are dominated by detrital fragments of quartz plus potassic feldspar plus or minus plagioclase, occasionally with myrmekitic structures, and by perthitic potassic feldspar. All of these fragments clearly point to felsic plutonic rocks in the pertinent source area. In addition, as opposed to sample S1, samples S2–S5 contain large amounts of bioclasts, while the content in metamorphic minerals is invariably low. All of the samples including sample S1 contain small amounts of glassy volcanic fragments.

Throughout the section, paleocurrent directions, based on cross-beds, pebble imbrication, groove casts, flute casts and ripple crest orientations consistently indicate south-directed paleoflow (Fig. 2C,E). We interpret
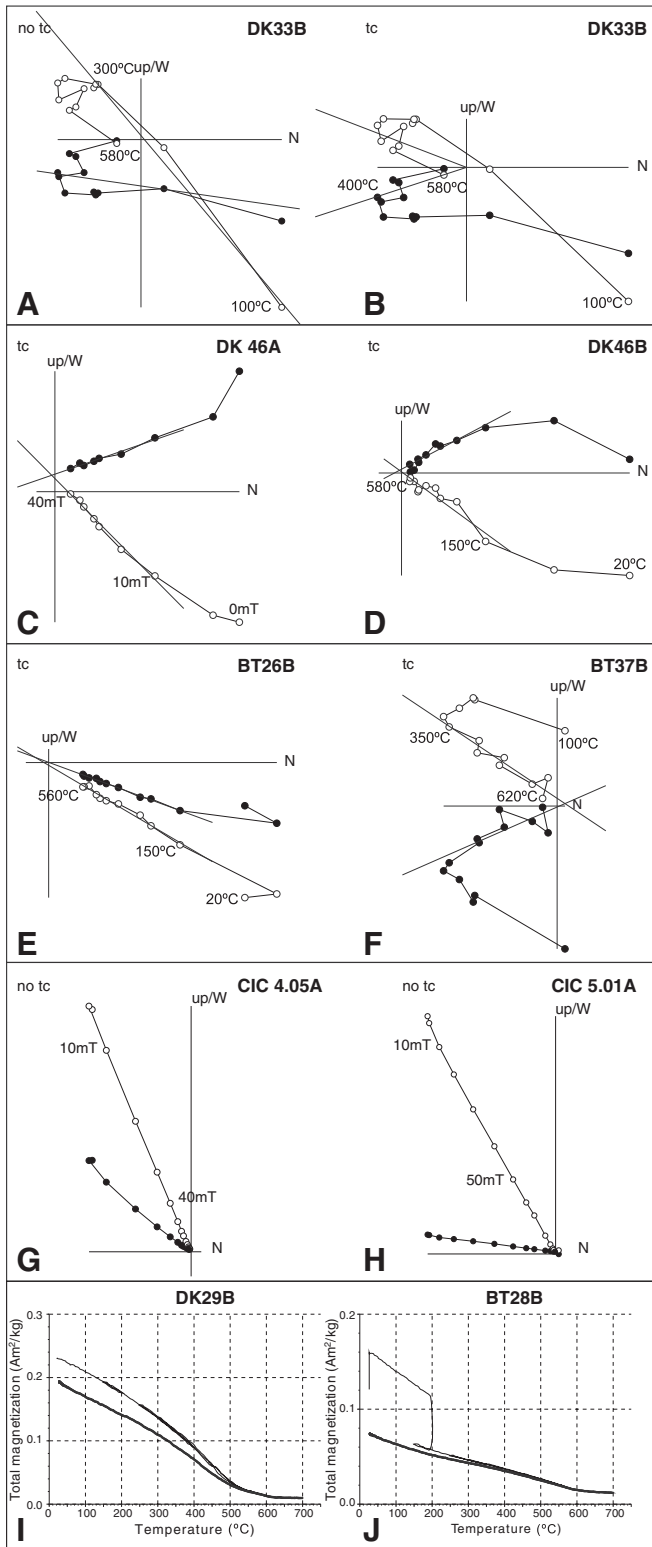
Fig. 4. a–h: Orthogonal vector diagrams showing characteristic demagnetization diagrams for representative sampled sites. Closed (open) circles indicate the projection on the horizontal (vertical) plane. Alternating field and thermal demagnetization steps are indicated. All diagrams (except for diagram a) are displayed after tilt correction (tc); i–j: thermomagnetic curves measured on a Curie balance (Mullender et al., 1993) for section 1 (DK) and section 2 (BT). Red (blue) curves represent the heating (cooling) curves.

section 1 as a regressive sequence from marine nummulitic limestones, through a deltaic, into a fluvial system, which becomes coarser, and hence more proximal to the top.

The northern limb of the Çiçekdağı syncline with its subvertical bedding orientation (Fig. 2) shows a similar stratigraphic sequence, but it is thinner and is characterized by well-developed progressive angular unconformities (Fig. 2G). The dips of the units below the unconformities are always higher than the dips of the overlying units, showing evidence for cycles of synsedimentary tilting, erosion, and renewed deposition (cf. Riba, 1976). In other words: these intraformational unconformities demonstrate that the northern flank of the Çiçekdağı syncline underwent tilting, erosion and renewed deposition, whereas at the same time deposition in the southern flank of the syncline was continuous and thus demonstrates synsedimentary formation of the Çiçekdağı syn- and anticline.

To the north of the Akçakent high, a lithostratigraphy is exposed that is similar to the lower parts of the Çiçekdağı basin, but differs higher in the section (Fig. 2A,F). Comparable to the south, in the southern flank of Yerköy syncline the lower part of the section contains frequent cross-bedded, lense-shaped red sandstones and conglomerates with southward paleocurrent directions. Instead of a continuing coarsening-upward sequence, however, section 2 grades northward and upward into gypsum-bearing, cyclically-bedded red, blue and green lacustrine claystones. Notably, around ~120 m in the section, paleocurrent directions reverse by ~180°, and are northward throughout the top 200 m of the section (Fig. 2B,F).

3. $^{40}Ar/^{39}Ar$ geochronology

We collected a sample, C1, from a basaltic lava in a sequence that overlies the top of the basal black shales, and that stratigraphically underlies nummulitic limestones.

Sample C1 was crushed, sieved and washed in acetone and distilled water. The transformation $^{39}K(n, p)^{39}Ar$ was performed during irradiation at the IFE Kjeller reactor in Norway, using the Taylor Creek Rhyolite as flux monitor (28.619 ± 0.034 Ma; Renne et al., 2010). Samples were step heated in a Heine type double-vacuum oven at the Geological Survey of Norway. The extracted gases were swiped over getters (SAES AP-10) for 2 min, and then for 9 min in a separate part of the extraction line. The peaks were determined by peak hopping (at least 8 cycles) on masses ^{41}Ar to ^{35}Ar on a Balzers electron multiplier on a MAP 215-50 mass spectrometer. Data from unknowns were corrected for blanks prior to being reduced with the IAAA software package (Interactive Ar–Ar Analysis, written by M. Ganerød, NGU Trondheim, Norway) that implements the equations in McDougall and Harrison (1999) using the decay constants of Renne et al. (2010) and the trapped $^{40}Ar/^{36}A$ ratio of 298.56 ± 0.31 of Lee et al. (2006). Data reduction in IAAA incorporates corrections for interfering isotopes (based on K_2SO_4 and CaF_2 salts included in the irradiation package), mass discrimination, error in blanks and decay of ^{37}Ar and ^{39}Ar.
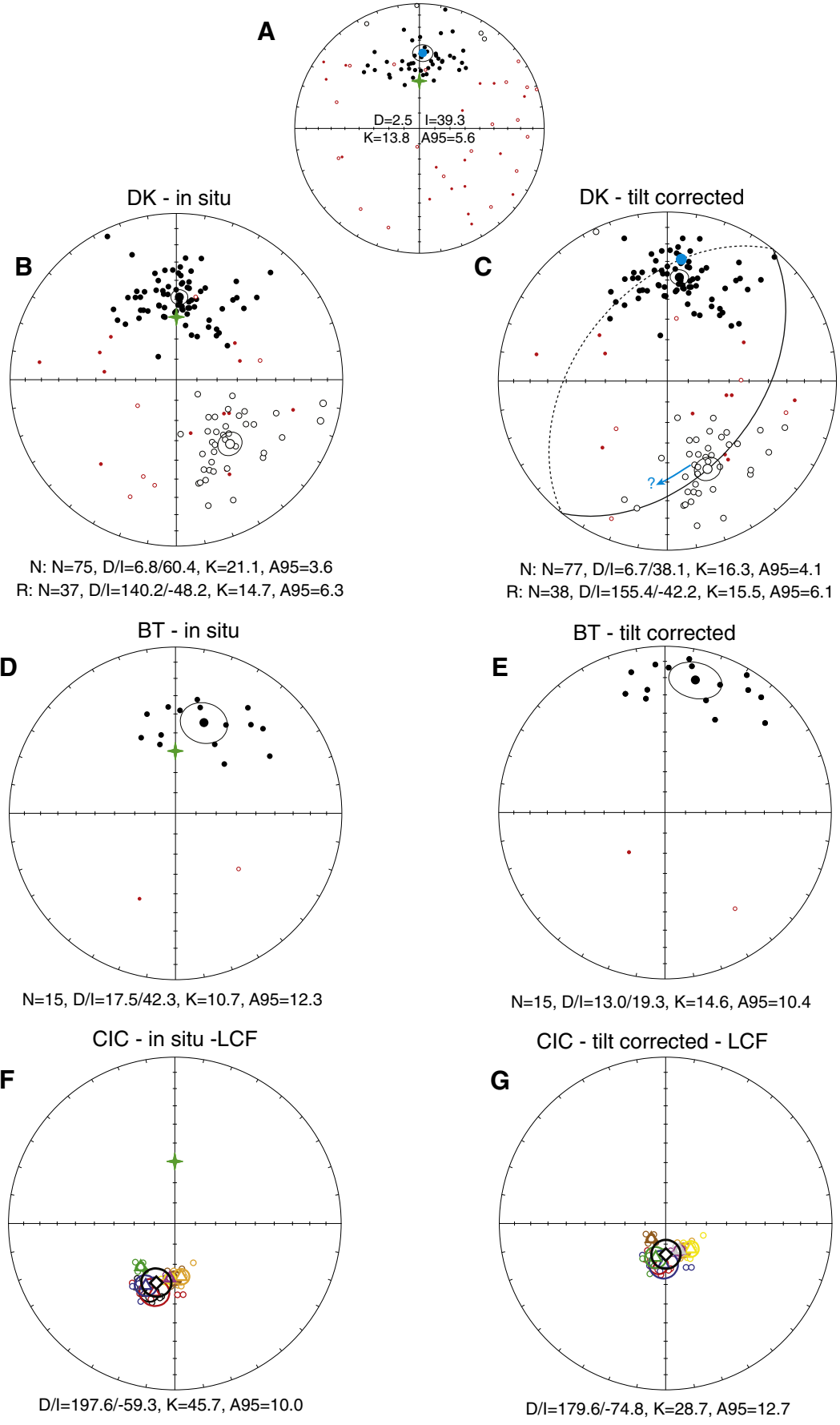
Analysis by the $^{40}Ar/^{39}Ar$ method yielded a disturbed spectrum without a valid plateau age (Fig. 3). The weighted mean age for the most stable part of the spectrum (steps 2–10) is 48.88 ± 1.95 Ma (2σ). Isochron ages calculated for parts of the spectrum are 52.85 ± 1.33 Ma (2σ) and 45.05 ± 1.82 Ma (2σ), but this is for only 33.3% and 23.1% of the cumulative ^{39}Ar respectively. Nevertheless, these data are compatible with the Lutetian age of the overlying shallow marine limestones (48.6–40.4 Ma, Luterbacher et al., 2004).

4. Paleomagnetism

4.1. Paleomagnetic sampling

We collected samples for paleomagnetic analysis from two localities in the Çiçekdağı Basin. Section 1 (codes DK) was sampled for

DK- low T / LCF component - in situ

A

D=2.5   I=39.3
K=13.8   A95=5.6

DK - in situ

B

N: N=75, D/I=6.8/60.4, K=21.1, A95=3.6
R: N=37, D/I=140.2/-48.2, K=14.7, A95=6.3

DK - tilt corrected

C

N: N=77, D/I=6.7/38.1, K=16.3, A95=4.1
R: N=38, D/I=155.4/-42.2, K=15.5, A95=6.1

BT - in situ

D

N=15, D/I=17.5/42.3, K=10.7, A95=12.3

BT - tilt corrected

E

N=15, D/I=13.0/19.3, K=14.6, A95=10.4

CIC - in situ -LCF

F

D/I=197.6/-59.3, K=45.7, A95=10.0

CIC - tilt corrected - LCF

G

D/I=179.6/-74.8, K=28.7, A95=12.7

magnetostratigraphy. The top 609 m was sampled at 95 levels. The section overlies the Lutetian nummulitic limestones conformably (Fig. 2). The interval between the Lutetian nummulitic limestones and the base of the sampled interval has a stratigraphic thickness of ~380 m. The samples were collected from 45 levels in section 2 (site BT) in the northern flank of the Çiçekdağı anticline, and from eight Eocene lavas (dated in the previous section) in the core of the Çiçekdağı anticline (sites CIC) to test vertical axis rotations. Sampling occurred with a gasoline powered motor drill. A large part of the sampled cores provided two standard specimens. Sample orientations were measured with a magnetic compass. Sample orientations and measured bedding planes were corrected for 004.8°E declination.

4.2. Paleomagnetic analysis

Specimens were demagnetized using alternating field (AF) and thermal (TH) progressive stepwise demagnetization. Specimens were thermally demagnetized in a magnetically shielded oven, with steps of 20–50 °C, up to a maximum of 680 °C and measured on a 2G DC SQUID cryogenic magnetometer. We carried out AF demagnetization, using an in-house developed robot assisted and fully automated 2G DC SQUID cryogenic magnetometer. Demagnetization was carried out in increments of 5–10 mT, up to a maximum of 90 mT. Specimens from section 1 (DK) were demagnetized thermally as well as using AF demagnetization. Specimens from site BT were all demagnetized thermally, whereas all CIC samples were demagnetized using AF demagnetization.

Thermomagnetic runs were carried out to determine the magnetic carriers in the rock samples. The runs were carried out in air, using a modified horizontal translation type Curie balance, with a sensitivity of ~5×10^{-9} Am^2 (Mullender et al., 1993) (Fig. 4). Approximately 50 mg of rock powder was put in a quartz glass sample holder and hold in place by quartz wool. Heating and cooling rates were 10 °C/min. Temperatures were increased to a maximum of 700 °C.

Demagnetization diagrams of the natural remanent magnetization (NRM) were plotted as orthogonal vector diagrams (Zijderveld, 1967) (Fig. 4). We used principal component analysis (Kirschvink, 1980) to determine the characteristic remanent magnetization (ChRM) directions. In a limited number of cases (10 specimens out of the total number of samples used for the calculation of the mean ChRM of section 1 (DK)) we used the great-circle approach (McFadden and McElhinny, 1988) on samples that deviated from the general NRM behavior. This method can be used to identify the direction on the great circle that lies closest to the average direction obtained from well-determined NM directions.

To calculate site and virtual geomagnetic pole (VGP) means we used Fisher statistics (Fisher, 1953). Secular variation of the Earth's magnetic field induces scatter in paleomagnetic directions. Because this scatter is near-Fisherian at the poles, but gradually becomes more elongated towards the equator (Creer, 1962; Tauxe and Kent, 2004), we calculated VGPs from all directions. Subsequently a fixed 45° cut-off was applied to remove outliers from the datasets and the errors in declination and inclination were calculated (ΔD_x and ΔI_x, respectively). For site CIC, we used the common true mean direction (CTMD) test developed by McFadden and McElhinny (1990) to determine whether distributions share a CTMD. We use the test and their classification (A, B, C and indeterminate) based on the critical angle γ_c and the angle γ between the means. We use the CTMD test

with simulation, which is essentially equivalent to using the V_w parameter of Watson (1983).

Paleomagnetic data derived from sediments are often affected by inclination shallowing, caused by compaction during burial. We applied the elongation/inclination (E/I) method of Tauxe et al. (2008) on the results from section 1 (DK, after application of a 45° cut-off on the VGPs), which is based on the TK03.GAD model (Tauxe and Kent, 2004). The model is based on the assumption that the field averaged over sufficient time resembles that of a geocentric axial dipole (GAD). To apply the model successfully, a relatively large number of individual directions is required (preferably N > 100).

4.3. Paleomagnetic results

4.3.1. ChRM and rock magnetism

A total number of 133 specimens were demagnetized from section 1 (DK). Initial intensities typically range ~5–275 mA/m. We carried out alternating field and thermal demagnetization on the specimens. Both techniques gave similar results (Fig. 4). The main magnetic carrier in the samples is magnetite (Fig. 4). The thermomagnetic curve shows little alteration during heating and the curve represents for nearly 50% paramagnetic behavior. The thermomagnetic curve also indicates the presence of maghemite or hematite between 530 °C and ~615 °C. Regarding the red color of the sampled sediments and the remaining ~15% of magnetization that remains in the specimens after AF demagnetization, we find it likely that hematite is this magnetic carrier. In 86 specimens we identified a low coercive force (LCF) or low temperature (LT) secondary component. This was identified between ~0–10/15 mT and temperature ranges up to a maximum of 250 °C (e.g. Fig. 4a). This LCF/LT component is quite scattered (Fig. 5a). After application of the 45° fixed cut-off, the mean LCF/LT component is: D = 2.5°/I = 39.3°. This direction is too shallow to be of a present-day field origin. We identified the high temperature (HT, until ~580 °C) and high coercive force component (HCF, until ~60 mT) as the ChRM direction (Fig. 4b–d). In ~35% of the specimens this is a reversed component and the section is thus dominated by normal polarity intervals. The mean ChRM directions of the normal and the reversed component do not pass the reversal test (McFadden and McElhinny, 1990), and mean ChRM directions for both polarities after tilt correction are D = 155.4°/I = −42.2° and D = 6.7°/I = 38.1° (Fig. 5b–c). We address this to the presence of the LCF/LT overprint. This direction is near-parallel to the normal directions of the HCF/HT component (Fig. 5c) and therefore hardly affecting the normal polarity specimens, but partially overprinting the reversed signal (Fig. 5c). From the normal polarity data, we conclude that the section experienced no significant rotation after deposition.

The demagnetized specimens of section 2 (BT) all yield normal polarities except for one specimen (Fig. 4e–f). In total, 24 specimens were demagnetized. Initial intensities range ~20–230 mA/m. All samples were demagnetized thermally (Fig. 4e–f). The main magnetic carrier in the samples is magnetite (Fig. 4j). The thermomagnetic curve shows remarkably little alteration during heating and represents for 50% paramagnetic behavior. Between 585 °C and ~650 °C there is a small remaining magnetization that most probably represents hematite (650 °C is too high for the presence of maghemite).

We demagnetized 56 specimens from eight lava flows using AF demagnetization. Initial intensities range 0.3–5 MA/m. All demagnetized specimens from site CIC yield reversed polarities (Fig. 4g–h). The orthogonal vector diagrams show two different components in the lavas, one demagnetizing between 10 and 40 mT and a second one in the 50–

Fig. 5. a) In situ low temperature/low coercive force (LT/LCF) component of section DK. Blue circle indicates the mean LT/LCF direction and its cone of confidence (α_{95}). b–g) In situ and tilt corrected ChRM directions of sections 1 and 2 (DK and BT respectively). c) Blue circle indicates the mean LCF/LT component after tilt correction. Great circle through the reversed polarity mean and the LCF/LT component mean indicates (blue arrow) where the reversed polarity directions probably originally were located. f–g) Individual site directions and 6-site mean result from the CIC lavas. Open (closed) symbols denote projection on upper (lower) hemisphere. Green star indicates the GAD field direction at the current latitude. Large black/white symbols with black circle indicate respectively the mean directions and their cone of confidence (α_{95}). Red (small) circles indicate the individual directions rejected after applying a 45° fixed cut-off on the VGP directions.

70 mT interval (Fig. 4g–h). The mean of the higher coercive force component has very high k-values, suggesting it is a secondary overprint. We therefore identified the low coercive force component (demagnetizing between 10 and 40 mT) as the primary ChRM direction.

4.3.2. Magnetostratigraphy of section 1

We constructed a polarity pattern (Fig. 6) for section 1 (DK). Below the section, nummulitic limestones that are Lutetian in age are exposed, followed by a 380 m unexposed part until the start of the section, which are underlain by volcanics from which we determined a weighted mean age of 48.88 ± 1.95 Ma. Given the continuity of the section from the Lutetian limestones onward, we explored the oldest possible magnetostratigraphic correlations in or after the Lutetian. To date section 1, we correlated the constructed reversal pattern (Fig. 6) to the Global Polarity Time Scale (GPTS) (Fig. 7). The correlated interval has to postdate the age of the volcanics underlying the section (48.88 ± 1.95 Ma) and correspond to a period in the GPTS that is dominated by normal polarities. This resulted in two possible correlations in the Bartonian–Priabonian interval, in the interval between ~39 and 35 Ma of the GPTS (Luterbacher et al., 2004). The corresponding sedimentation rates for both correlations are 12.2 cm/kyr and 20.0 cm/kyr (Fig. 7). In both cases, this would give a Bartonian–Priabonian (late Eocene) age to the studied section. The displayed correlations would suggest a time span of approximately 2 to 4 Myrs for the entire section. An alternative correlation to the Oligocene (Rupelian–Chattian) would also reasonably well correlate to our polarity pattern. This would, however, imply a large sedimentation rate difference between the unexposed part (between the limestones and the start of the measured section) and the measured section, or the presence of a hiatus. We therefore render this third correlation unlikely.

At the time of deposition of the sediments in the Çiçekdağı Basin, we would expect a position of the CACC at the southern Eurasian margin. However, the calculated paleolatitudes from the normal and reversed polarity data are very low. Therefore, we applied the E/I method on the normal polarity data from section 1 (DK), because the normal and reversed polarity data sets do not share a common true mean direction. Application of the method to the normal polarity data is favored, because we argue that the reversed polarity data are affected by a LCF/LT overprint. Correction for inclination shallowing results in a significant correction of the paleolatitude from λ = 21.4° to λ = 41.4° (Table 1, Fig. 8) which fits within error with expected Eurasian values, supporting a primary paleomagnetic signal. We should mention however, that the number of specimens is lower (N = 75) than the desired number of N > 100.

4.3.3. Vertical axis rotation analysis

The normal magnetic field component of section 1 has a declination of 6.8 ± 4.8°, which gives a negligible rotation compared to the expected direction of 5.4 ± 3.4° based on the APWP of Torsvik et al. (2008). The mean of the identified ChRM directions before and after tilt correction for site BT is displayed in Fig. 5d,e. The in situ mean ChRM direction is clearly no present-day field overprint. The tilt corrected mean ChRM direction (D = 13.0° ± 10.6°/I = 19.3° ± 19.1°, Table 1) shows a statistically insignificant deviation from the expected direction. We suggest that the low inclination is the result of compaction-induced inclination shallowing, but the limited number of demagnetized specimens does not allow correcting using the E/I method.

A Common True Mean Direction (CTMD) test (McFadden and Lowes, 1981) on all mean ChRM directions of the CIC lava sites, revealed that two times two lava flows share a CTMD with classification A (between flows 5 and 6, $G_c = 4.9 > G = 3.4$ and between flows 7 and 8. $G_c = 3.1 > G = 0.1$). Therefore, we reinterpreted the site by grouping the presumed flows with a CTMD, resulting from the presence of six flows with statistically different directions (Table 1). The mean of the identified ChRM directions is displayed in Fig. 5f–g. The six lava sites of CIC provide a tilt-corrected direction of D = 179.7 ±

27.4.1°/I = −74.8 ± 7.7°, showing a non-significant deviation from the expected declination.

One earlier paleomagnetic study has been carried out in the Çiçekdağı area (see Fig. 2 for location). Sanver and Ponat (1981) presented paleomagnetic data from volcanic rocks of probably early Eocene age. The derived tectonic rotation of 31.3º ± 24.8° CCW (we recalculated the error in declination, ΔD_x following procedures of Deenen et al. (2011)) is larger than (and opposite to) the calculated rotations from our data sets. Given the large error in declination (± 24.8°) and age uncertainty in the study of Sanver and Ponat (1981), we therefore conclude from our data that the study area has most likely not experienced a significant vertical axis rotation episode after deposition. The paleocurrent directions we measured in our sections have therefore not been modified by younger tectonic rotations.

5. Discussion

5.1. Basin evolution

A noteworthy characteristic of the Çiçekdağı Basin is that its basement in the south – the high-grade CAM – is of different metamorphic grade than its basement to the north — the supra-subduction zone type Çiçekdağı Ophiolite (Fig. 2). We compare the basin evolution above these two basement units.

Given their proximity, we assume that the nummulitic limestone (Fig. 2A,D) can be regarded as a timeline. Along the southern contact of the Çiçekdağı Basin with the CACC, this limestone marker is only ~20 m thick, and is underlain by conglomerate patches consisting of proximal CACC debris. To the north of Çiçekdağı syncline, overlying the Çiçekdağı Ophiolite, however, the limestones are thicker (~50 m), and the 200 m thick underlying sequence contains Eocene lavas as well as shallow marine, shell-bearing black shales. During the early stages of basin formation, the CACC thus formed the southern basin margin, and accommodation space increased to the north. Sediments were in situ (limestones) or locally derived (minor clastics, volcanics), or sourced from the south, as seen in conglomerates below the limestones with CACC debris at the southern margin.

The transition from nummulitic limestones into red fluvial clastics was gradual, as we described for the base of section 1. However, the sediment petrography data show that the sediments of the Çiçekdağı syncline contain e.g. glaucophane, suggesting HP-LT metamorphic rocks were eroded. This HP mineral is unknown from the CACC, but have been described in e.g. the Cretaceous and older massifs to the north of the CACC (Okay et al., 2006). This is consistent with the paleocurrent directions (Fig. 2), and suggests that the Çiçekdağı sediments were at least partly derived from sources to the north of the Çiçekdağı anticline, most likely, in the Pontides, or perhaps the İzmir–Ankara suture zone, where HP metamorphic rocks have been reported (e.g., Okay et al., 2006). In other words, during deposition of the rocks of sample S1, the Çiçekdağı basin was connected to a hinterland (far) to the north of the CACC.

Finally, the reversal in paleocurrent directions to northward paleoflow along the northern limb, and the intra-formational angular unconformities in the southern subvertical limb of the Çiçekdağı anticline provide clear evidence that shortly after the onset of red bed sedimentation, folding, thrusting and uplift of the Çiçekdağı anticline started, sometime between ~38 and 35 Ma. The coarsening-upward sequence in the southern section 1 is consistent with erosion of the Akçakent high — further illustrated by reworking of nummulitic limestones in the higher part of the section (samples S2–5, Fig. 2F). The northern section 2 shows a gradual change northward into a lacustrine environment. We interpret this change to result from accumulation of water from the north in front of a rising topographic barrier related to the development of the Akçakent high.

The Çiçekdağı Basin therefore provides evidence (detrital glaucophane) that the first arrival of sediment from (north of) the
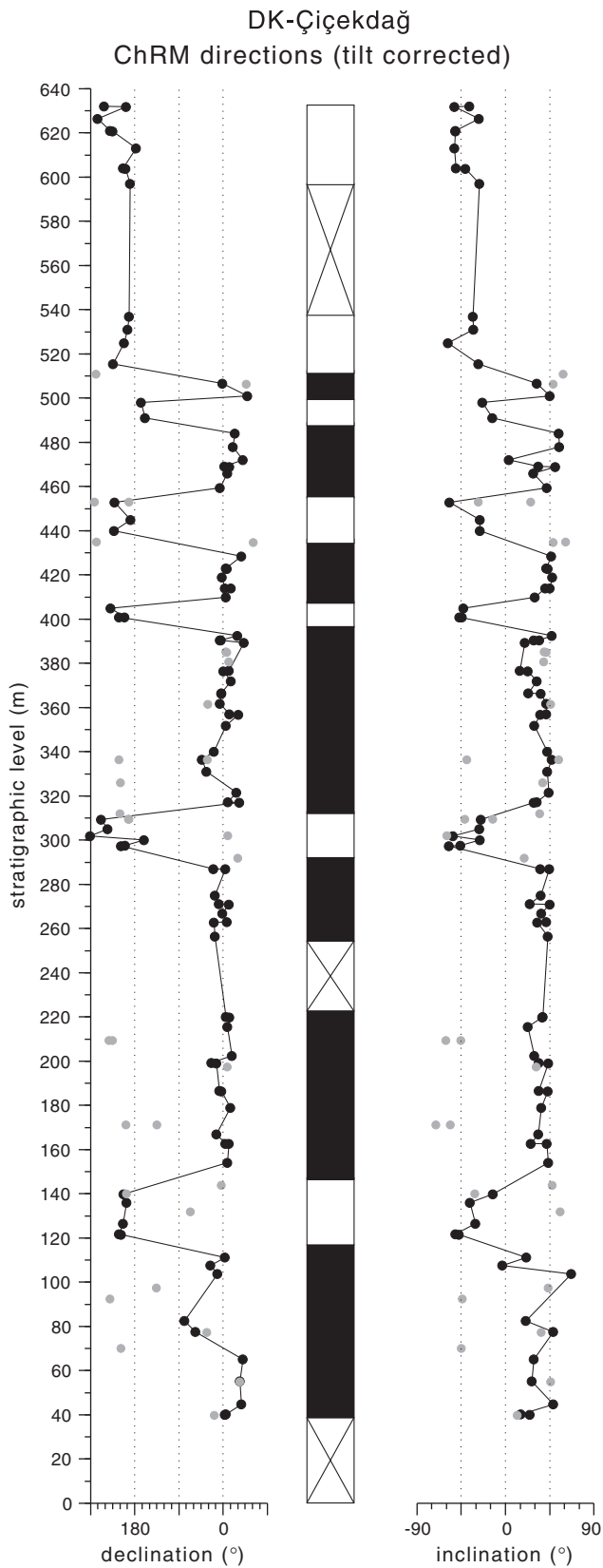
DK-Çiçekdağ
ChRM directions (tilt corrected)

Fig. 6. Figure showing the stratigraphic level versus the declinations and inclinations of all interpreted ChRM directions for section 1 (DK) and the derived polarity pattern. Gray circles show uncertain data.

İzmir–Ankara suture onlapping onto exhumed CACC basement occurred around ~38–35 Ma (Fig. 7), shortly followed by folding. Prior to red bed sedimentation, the Çiçekdağı Basin unconformably covered ophiolites to the north and CACC basement to the south.

5.2. Context of compression: connection to the Çankırı Basin

In a recent paper, Genç and Yurur (2010) argued that compressional deformation found in the center and along the periphery of the CACC, including the Çiçekdağı area (referred as the Mahmutlu zone), occurred coevally with extensional detachments unroofing the CACC. They proposed an extensional collapse scenario of a gravitationally unstable CACC driven by internal excess gravitational potential energy. We consider such a scenario unlikely. Among other arguments (see Lefebvre et al., 2012 for discussion), the compressional deformation in the Çiçekdağı Basin definitely postdates deposition of the Eocene limestones that unconformably cover already exhumed CACC basement. The documented extensional detachments (Gautier et al., 2002, 2008; Lefebvre et al., 2011, submitted for publication) and dated extensional shear zones (Isık, 2009; Isık et al., 2008) that exhumed CACC basement are all late Cretaceous to perhaps early Paleocene in age (~75–60 Ma), i.e. much older than the late Eocene deformation documented here. There are no documented major extensional structures of Eocene age. Therefore, there is no evidence that extensional unroofing of the CACC and compression along its perimeter and center were coeval: instead, all evidence suggests that extensional detachment faulting exhuming CACC predates the Eocene (and elsewhere perhaps younger) compressional deformation. Some high-angle normal faults are active today and may date back to the late Miocene (Göncüoğlu et al., 1993), but no convincing evidence has been presented that documents continuous extensional deformation from late Cretaceous to the Present as postulated by Genç and Yurur (2010).

We therefore explore the late Eocene compressional deformation and sedimentation history of the Çiçekdağı Basin within the context of regional basin evolution. The red bed successions from the Çiçekdağı Basin are exposed on a regional scale, and can be followed ~100 km northward into the Çankırı Basin (Kaymakcı et al., 2009). The Çankırı Basin straddles the boundary between the Pontides and the CACC, which below the southern Çankırı Basin consists of upper Cretaceous ophiolites intruded by upper Cretaceous granitoids, fringed by Ankara mélange of the suture zone. The upper Cretaceous part of the Çankırı Basin stratigraphy has been described as a forearc basin. This forearc basin was restricted to the southern margin of the Pontides and does not reach the CACC (Kaymakcı et al., 2009). From Paleocene time onwards, however, sediments derived from the Pontides started to straddle the boundary between the Pontides and the northern CACC during continuous thrusting, which led Kaymakcı et al. (2009) to conclude that the Cretaceous forearc basin related to northward subduction below the Pontides transformed into a southward expanding foreland basin succession as a result of collision between the CACC and the Pontides (Fig. 9). This time interval coincides with the formation of a northward convex orocline in the Pontides, providing further evidence for a Paleocene CACC–Pontide collision (Kaymakcı et al., 2003b; Meijers et al., 2010a).

The non-marine foreland basin sedimentation, shortly followed by south-directed thrusting and folding, migrated southward, arriving in the Çiçekdağı Basin ~38–35 Ma ago as shown by the syn-sedimentary folding in our magnetostratigraphically dated section 1 (Fig. 9). The evolution of the Çiçekdağı Basin can therefore well be explained by the incorporation of CACC into the Paleocene–Eocene collision zone between the CACC and the Pontides. This history is similar to that proposed by Keskin et al. (2008), although they dated the end of subduction, based on their preferred scenario to explain regionally extensive volcanic rocks, around 42 Ma. Similarly, Görür et al. (1998) considered the Eocene compressional recorded in basins such as the
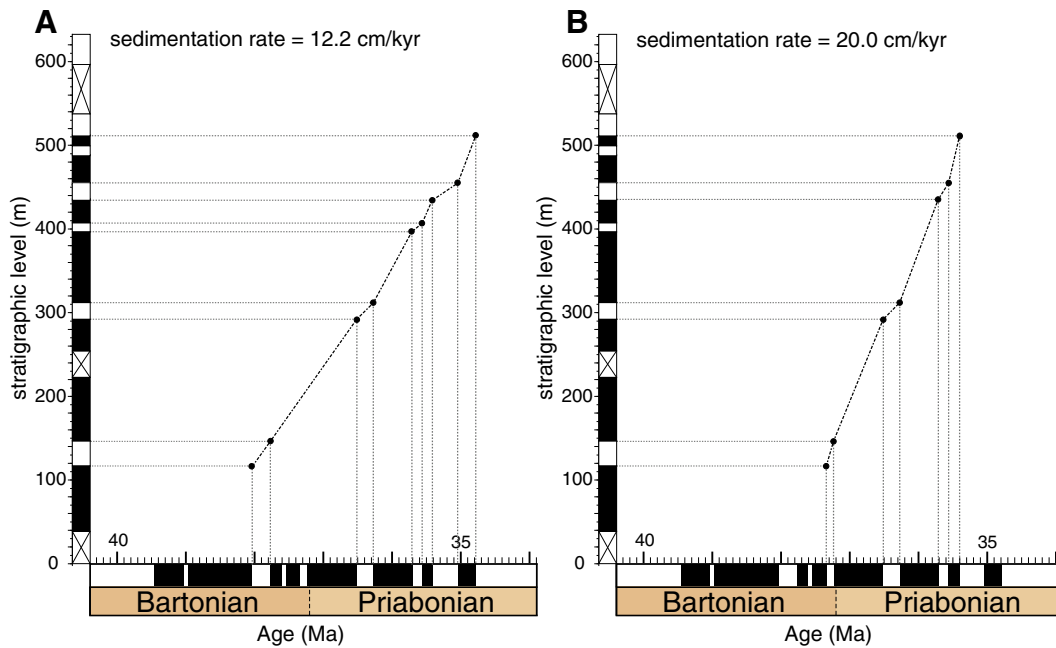
Fig. 7. a) and b) show the relation between the stratigraphic level and the age in Ma for both correlations. Both correlations show a relatively constant sedimentation rate through time.

Çiçekdağı Basin to result from collision at a larger scale between the Taurides and the Pontides, with the CACC between the colliding blocks undergoing a complex compressional and rotational evolution. The data we present in this paper cannot shed light on the regional tectonic evolution of the CACC, but we concur that the ~38–35 Ma compression we argue for in the Çiçekdağı Basin is related to an overall collisional setting, probably during the late stages of collision. However, an older tectonic history juxtaposing the high-grade metamorphic rocks of the CACC and the Ankara ophiolitic mélange must have preceded this basin history.

5.3. Relationship between the CAM and CAO below the Çiçekdağı syncline

The sediments exposed in the Çiçekdağı syncline cover a contact between the non- to low-grade metamorphic mid-Cretaceous ophiolites of the Akçakent high, and the high-grade metasediments of the CACC, which is E–W oriented and continuous over a distance of >50 km. Because the mid-Cretaceous ophiolites are structurally higher in the tectonostratigraphic sequence than the CACC metamorphic rocks, but contain a thicker Lutetian and older sedimentary sequence, they must have been at a lower topographic level at the onset of Eocene sedimentation. This is most straightforwardly explained by a hypothetical pre-Eocene structure hidden below the Çiçekdağı syncline with a northward normal component of motion, or alternatively an E–W trending strike-slip fault below the basin. Regardless of the nature of the structure below the Çiçekdağı syncline, our analyses demonstrate that exhumation of the CACC, at least locally associated with extensional detachments (Gautier et al., 2002, 2008; Lefebvre et al., 2011, submitted for publication), predates the first arrival of sediments derived from the Pontides and İzmir–Ankara suture zone, and also predates the southward migrating compression associated with the collision of the CACC with the Pontides.

5.4. Plate tectonic implications

Extensional detachments in central Anatolia and the Mediterranean region, exhuming high-grade metamorphic rocks are widespread in the Mediterranean region (Bozkurt and Oberhänsli, 2001; Jolivet et al.,

2009; Tirel et al., 2009; van Hinsbergen, 2010; Vissers et al., 1995). These regions seem exclusively positioned in an overriding plate above a subduction zone, with extension generally ascribed to roll-back of the subducting slab, and high-temperature metamorphism to interaction of overriding plate crust with asthenosphere in the mantle wedge (e.g., Jolivet et al., 2009). The regional high-temperature metamorphism (e.g. Whitney et al., 2001), widespread magmatism (e.g. Kadıoğlu et al., 2003), extension and exhumation (Gautier et al., 2008; Lefebvre et al., 2011, submitted for publication) and the intra-Tauride high-pressure belt in the south (Okay, 1984, 1986; Pourteau et al., 2010) (Fig. 1) seem to suggest that the CACC was also positioned in an overriding plate of a subduction zone during the late Cretaceous (Fig. 9).

The geology of the Çiçekdağı and Çankırı Basins, however, clearly demonstrates that extension in the CACC associated with the exhumation its upper Cretaceous crystalline rocks predates collision of the CACC with the Pontides. The late Cretaceous volcanic arc on the Pontides (Boztuğ and Harlavan, 2008; Okay et al., 2001; Tüysüz et al, 1995) and the late Cretaceous to perhaps early Paleocene Çankırı forearc basin evolution (Kaymakcı et al., 2009; Rice et al., 2006) attest to the Cretaceous to Paleocene northward subduction below the Pontides of a plate that since the late Cretaceous contained the CACC (see also Keskin et al., 2008). This must, therefore, have been a separate plate from Eurasia and Africa, which was an overriding plate with respect to the intra-Tauride subduction zone and an downgoing plate with respect to the Pontides until Paleocene–Eocene collision (Fig. 9).

6. Conclusions

In this paper, we study the sedimentary, stratigraphic and tectonic evolution of the Çiçekdağı Basin, which is located in the northwestern part of the CACC in central Turkey. The basin unconformably overlies high-grade metamorphic basement of the CACC in the south, and low-grade to non-metamorphic Central Anatolian Ophiolites to the north, which were emplaced over the metamorphic rocks of the CACC in late Cretaceous time. Sedimentation of the basin postdates exhumation of the high-grade metamorphic rocks of the CACC.

Table 1

Paleomagnetic data from the Çiçekdağı Basin. N_a = number of specimens analyzed, N_{45} = number of specimens remaining after application of the 45° fixed cut-off on the VGPs, dec = declination, inc = inclination, k = estimate of the precision parameter determined from the ChRM directions, α_{95} = 95% cone of confidence of the ChRM directions, K = precision parameter estimated from the virtual geomagnetic poles (VGPs), A95 = cone of confidence determined from the mean VGP direction. $A95_{min}$ and $A95_{max}$ are the minimum and maximum possible estimates of the A95 for the given data sets after Deenen et al. (2011). DK LT/LCF = low temperature/low coercive force component, R = reversed component, N = normal component, DK N TK03 = mean of the DK data set after applying the E/I method.

| Site	NOTC																TC															
	N_a	N_{45}	N_s	dec	inc	k	α_{95}	k	$A95$	$A95_{min}$	$A95_{max}$	λ	ΔD_x	ΔI_x			N_a	N_{45}	N_s	dec	inc	k	α_{95}	k	A95	$A95_{min}$	$A95_{max}$	λ	$A95_{max}$	λ	ΔD_x	ΔI_x
DK LT/LCF	86	50	–	2.5	39.3	12.2	6.0	13.8	5.6	3.6	7.0	22.3	6.1	7.8			86	51	–	6.6	28.3	11.8	6.1	15.3	5.3	3.5	6.9	15.1	5.5	8.8
DK R	43	37	–	140.2	−48.2	17.4	5.8	14.7	6.3	4.0	8.4	29.2	7.2	7.4			43	38	–	155.4	−42.2	16.2	5.9	15.5	6.1	4.0	8.3	24.4	6.7	8.1
DK N	88	75	–	2.1	48.9	18.4	3.9	14.2	4.5	3.0	5.4	29.8	5.2	5.2			88	77	–	6.7	38.1	17.3	4.0	16.3	4.1	3.0	5.3	21.4	4.4	5.9
DK N TK03																	88	77	–	6.8	60.4	34.2	2.8	21.1	3.6	3.0	5.3	41.4	4.8	3.1
BT	17	15	–	17.5	42.3	13.8	10.7	10.7	12.3	5.8	14.9	24.5	13.5	16.2			17	15	–	13.0	19.3	13.7	10.7	14.6	10.4	5.8	14.9	9.9	10.6	19.1
CIC 8 flows HC	56	55	8	189.3	−61.3	279.3	3.3	136.8	4.8	3.4	6.6	−42.4	6.5	4.1			56	55	8	167.4	−75.4	126.8	4.9	38.8	9.0	3.4	6.6	62.5	19.8	5.4
CIC 8 flows LC	56	55	8	193.9	−60.4	94.0	5.7	46.4	8.2	3.4	6.6	41.4	11.0	7.1			56	55	8	171.3	−75.1	94.0	5.7	29.6	10.4	3.4	6.6	62.0	22.6	6.2
CIC 6 flows HC	56	55	6	197.6	−59.3	90.7	7.1	45.7	10.0	3.4	6.6	40.1	13.1	8.9			56	55	6	179.7	−74.8	90.9	7.1	28.7	12.7	3.4	6.6	61.5	27.4	7.7
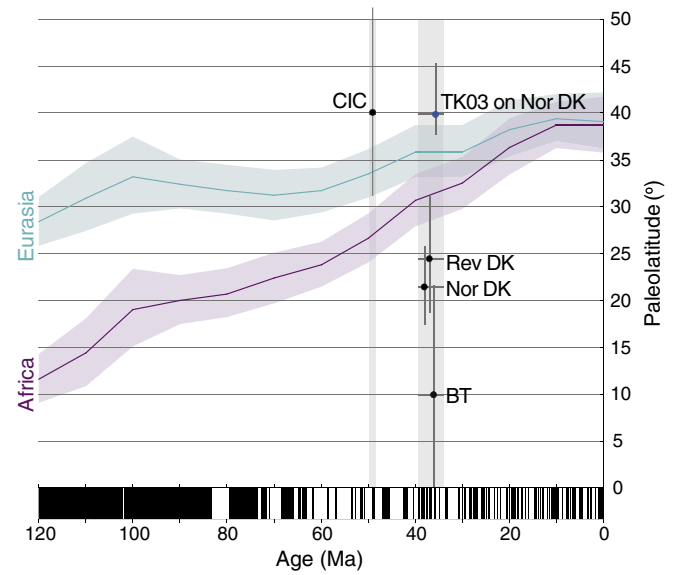
Fig. 8. Age versus latitude plots of all paleomagnetic data from this study. The normal and reversed polarity data of DK are indicated separately. In blue the E/I corrected paleolatitude for the normal polarity data of DK is indicated. Eurasian and African curves show the position of both continents at the position of the Çiçekdağı sites calculated from the APW path of Torsvik et al. (2008). Shaded areas represent the A95 error envelopes.

The stratigraphy of the Çiçekdağı Basin consists of red conglomerates, sandstones and siltstones, which overlie a sequence of nummulitic limestones. In the south, these are separated from the CACC metamorphics by a thin layer of conglomerates, whereas in the north, a ~200 m thick sequence of volcanics underlain by shallow marine black shales with abundant shell fossils (exposed in a quarry south of Çiçekdağı in the core of the anticline) separates the nummulitic limestones from the ophiolitic basement. We provide a magnetostratigraphic analysis of the series of red beds, which is consistent with a late Eocene age (somewhere between 38 and 35 Ma), consistent with a relatively poorly resolved weighted mean 48.88 ± 1.95 Ma $^{40}Ar/^{39}Ar$ age for volcanic rocks underlying the nummulitic limestones. Sediment petrography suggests that the Eocene deposits were derived from the Pontides and İzmir–Ankara suture to the north, and are similar to contemporaneous deposits in the Çankırı Basin.

The upper Eocene sediments were deformed into a syncline in the south and an anticline in the north. Progressive unconformities in the syncline, and a sudden, ~180° change in paleocurrent directions from southward to northward along the northern flank of the anticline demonstrate syn-sedimentary folding of the Çiçekdağı Basin.

We interpret the folding to result from a gradual southward progression of foreland basin sediments, closely followed by folding, from the Çankırı Basin to the south, as a result of ongoing collision between the CACC and the Pontides.

Supplementary data to this article can be found online at http://dx.doi.org/10.1016/j.tecto.2012.07.003.
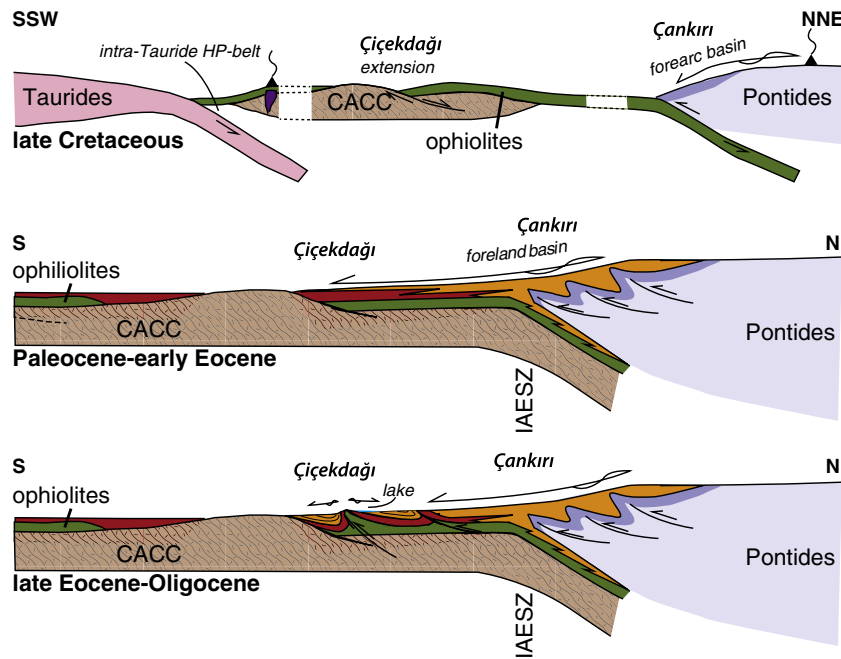
Acknowledgments

Fig. 9. Schematic model summarizing the role of the late Eocene syn-sedimentary compression in the Çiçekdağı Basin in the plate tectonic evolution of the CACC.

References

Akgün, F., Akay, E., Erdoğan, B., 2002. Tertiary terrestrial to shallow marine deposition in Central Anatolia: a palynological approach. Turkish Journal of Earth Sciences 11, 127–160.

Aydemir, A., Ateş, A., 2006. Structural interpretation of the Tuzgolu and Haymana Basins, Central Anatolia, Turkey, using seismic, gravity and aeromagnetic data. Earth, Planets and Space 2006, 951–961.

Bozkurt, E., Oberhänsli, R., 2001. Menderes Massif (Western Turkey): structural, metamorphic and magmatic evolution − a synthesis. International Journal of Earth Sciences 89, 679–708.

Boztuğ, D., Harlavan, Y., 2008. K–Ar ages of granitoids unravel the stages of Neo-Tethyan convergence in the eastern Pontides and central Anatolia, Turkey. International Journal of Earth Sciences 97, 585–599.

Boztuğ, D., Jonckheere, R.C., 2007. Apatite fission track data from central Anatolian granitoids (Turkey) constraints on Neo-Tethyan closure. Tectonics 26, TC3011, http://dx.doi.org/10.1029/2006TC001988.

Boztuğ, D., Tichomirowa, M., Bombach, K., 2007. ^{207}Pb–^{206}Pb single-zircon evaporation ages of some granitoid rocks reveal continent–oceanic island arc collision during the Cretaceous geodynamic evolution of the central Anatolian crust, Turkey. Journal of Asian Earth Sciences 31, 71–86.

Boztuğ, D., Güney, Ö., Heizler, M., Jonckheere, R.C., Tichomirowa, M., Otlu, N., 2009a. ^{207}Pb–^{206}Pb, ^{40}Ar–^{39}Ar and fission-track geothermochronology quantifying cooling and exhumation history of the Kaman–Kırşehir region intrusions, Central Anatolia, Turkey. Turkish Journal of Earth Sciences 18, 85–108.

Boztuğ, D., Jonckheere, R.C., Heizler, M., Ratschbacher, L., Harlavan, Y., Tichomirowa, M., 2009b. Timing of post-obduction granitoids from intrusion through cooling to exhumation in central Anatolia, Turkey. Tectonophysics 473, 223–233.

Clark, M., Robertson, A.H.F., 2005. Uppermost Cretaceous–Lower Tertiary Ulukisla Basin, south-central Turkey: sedimentary evolution of part of a unified basin complex within an evolving Neotethyan suture zone. Sedimentary Geology 173, 15–51.

Creer, K.M., 1962. The dispersion of the geomagnetic field due to secular variation and its determination for remote times from paleomagnetic data. Journal of Geophysical Research 67, 3461–3476.

Deenen, M.H.L., Langereis, C.G., van Hinsbergen, D.J.J., Biggin, A.J., 2011. Geomagnetic secular variation and the statistics of palaeomagnetic directions. Geophysical Journal International 186, 509–520.

Dilek, Y., Thy, P., 2006. Age and petrogenesis of plagiogranite intrusions in the Ankara mélange, central Turkey. Island Arc 15, 44–57.

Dirik, K., Göncüoglu, M.C., Kozlu, H., 1999. Stratigraphy and pre-Miocene tectonic evolution of the southwestern part of the Sivas Basin, Central Anatolia, Turkey. Geological Journal 34, 303–319.

Erdoğan, E., Akay, E., Ugur, M.S., 1996. Geology of the Yozgat region and evolution of the collisional Çankırı basin. International Geology Review 38, 788–806.

Erkan, E., 1976. Isogrades determined in the regional metamorphic area surrounding Kırşehir and their petrological interpretation (in Turkish with English summary). Yerbilimleri 2, 23–54.

Fisher, R.A., 1953. Dispersion on a sphere. Proceedings of the Royal Society of London A217, 295–305.

Floyd, P.A., Göncüoglu, M.C., Winchester, J.A., Yalınız, K.M., 2000. Geochemical character and tectonic environment of Neotethyan ophiolitic fragments and metabasites in the Central Anatolian Crystalline Complex, Turkey. In: Bozkurt, E., Winchester, J.A., Piper, J.D.A. (Eds.), Tectonics and Magmatism in Turkey and the Surrounding Area: Geological Society, London, Special Publications, pp. 183–202.

Frizon de Lamotte, D., Raulin, C., Mouchot, N., Wrobel-Daveau, J.-C., Blanpied, C., Ringenbach, J.-C., 2011. The southernmost margin of the Tethys realm during the Mesozoic and Cenozoic: initial geometry and timing of the inversion processes. Tectonics 30, TC3002, http://dx.doi.org/10.1029/2010TC002691.

Gautier, P., Bozkurt, E., Hallot, E., Dirik, K., 2002. Dating the exhumation of a metamorphic dome: geological evidence for pre-Eocene unroofing of the Nigde Massif (Central Anatolia, Turkey). Geological Magazine 139 (559–576).

Gautier, P., Bozkurt, E., Bosse, V., Hallot, E., Dirik, K., 2008. Coeval extensional shearing and lateral underflow during Late Cretaceous core complex development in the Nigde Massif, Central Anatolia, Turkey. Tectonics TC1003, http://dx.doi.org/10.1029/2006TC002089.

Genç, Y., Yurur, M.T., 2010. Coeval extension and compression in Late Mesozoic−recent thin-skinned extensional tectonics in central Anatolia, Turkey. Journal of Structural Geology 32, 623–640.

Gökten, E., Floyd, M.A., 2007. Stratigraphy and geochemistry of pillow basalts within the ophiolitic mélange of the İzmir–Ankara–Erzincan suture zone: implications for the geotectonic character of the northern branch of Neotethys. International Journal of Earth Sciences 96, 725–741.

Göncüoglu, M.C., Toprak, V., Kuscu, I., Erler, A., Olgun, E., 1991. Geology of the western part of the Central Anatolian Massif, part 1: southern section. Turkish Petroleum Corporation (TPAO) Report, 2909, pp. 1–140 (In Turkish).

Göncüoglu, M.C., Erler, A., Toprak, V., Yaliniz, K.M., Kuscu, I., Köksal, S., Dirik, K., 1993. Orta Anadolu Masifin batı bölümünün jeolojisi. Bolum 3: Orta Kızılırmak Tersiyer Baseninin jeolojik evrimi. T.P.A.O. Report, p. 3313.

Görür, N., Tüysüz, O., Sengör, A.M.C., 1998. Tectonic evolution of the Central Anatolian Basins. International Geology Review 40, 831–850.

Isık, V., 2009. The ductile shear zone in granitoid of the Central Anatolian Crystalline Complex, Turkey: implications for the origins of the Tuzgölü basin during the Late Cretaceous extensional deformation. Journal of Asian Earth Sciences 34, 507–521.

Isık, V., Lo, C.-H., Güncüoğlu, C., Demirel, S., 2008. ^{39}Ar/^{40}Ar ages from the Yozgat Batholith: preliminary data on the timing of Late Cretaceous extension in the Central Anatolian Crystalline Complex, Turkey. Journal of Geology 116, 510–526.

Jolivet, L., Faccenna, C., Piromallo, C., 2009. From mantle to crust: stretching the Mediterranean. Earth and Planetary Science Letters 285, 198–209.

Kadıoğlu, Y.K., Dilek, Y., Güleç, N., Foland, K.A., 2003. Tectonomagmatic evolution of bimodal plutons in the Central Anatolian Crystalline Complex, Turkey. Journal of Geology 111, 671–690.

Kaymakcı, N., White, S.H., van Dijk, P.M., 2000. Paleostress inversion in a multiphase deformed area: kinematic and structural evolution of the Çankırı Basin (central Turkey), part 1. In: Bozkurt, E., Winchester, J.A., Piper, J.A.D. (Eds.), Tectonics and Magmatism in Turkey and the Surrounding Area Geological Society London Special Publication, 173, pp. 445–473.

Kaymakcı, N., White, S.H., Dijk, P.M.V., 2003a. Kinematic and structural development of the Çankırı Basin (Central Anatolia, Turkey). A paleostress inversion study. Tectonophysics 364, 85–113.

Kaymakcı, N., Duermeijer, C.E., Langereis, C.G., White, S.H., Van Dijk, P.M., 2003b. Palaeomagnetic evolution of the Cankiri Basin (central Anatolia, Turkey):

implications for oroclinal bending due to indentation. Geological Magazine 140 (3), 343–355.

Kaymakcı, N., Özçelik, Y., White, S.H., van Dijk, P.M., 2009. Tectono-stratigraphy of the Çankiri Basin: late Cretaceous to early Miocene evolution of the Neotethyan suture zone in Turkey. In: van Hinsbergen, D.J.J., Edwards, M.A., Govers, R. (Eds.), Collision and Collapse at the Africa–Arabia–Eurasia subduction zone: Geological Society of London Special Publication, pp. 67–106.

Kaymakcı, N., Inceöz, M., Ertepınar, P., Koç, A., 2010. Late Cretaceous to recent kinematics of SE Anatolia (Turkey). In: Sosson, M., Kaymakcı, N., Stephanson, R., Bergarat, F., Storatchenoko, V. (Eds.), Sedimentary Basin Tectonics from the Black Sea and Caucasus to the Arabian Platform: Geological Society of London, Special Publication, 340, pp. 409–435.

Keskin, M., Genç, S.C., Tüysüz, O., 2008. Petrology and geochemistry of post-collisional Middle Eocene volcanic units in North-Central Turkey: evidence for magma generation by slab breakoff following the closure of the Northern Neotethys Ocean. Lithos 104, 267–305.

Ketin, I., 1955. Yozgat Bölgesinin Jeolojisi ve Orta Anadolu Masifinin Tektonik Durumu. Türkiye Jeoloji Kurumu Bülteni 6, 1–28.

Kirschvink, J.L., 1980. The least-squares line and plane and the analysis of palaeomagnetic data. Geophysical Journal of the Royal Astrological Society 62, 699–718.

Koçyiğit, A., Beyhan, A., 1998. A new intracontinental transcurrent structure: the Central Anatolian Fault Zone, Turkey. Tectonophysics 284, 317–336.

Lee, J.-Y., Marti, K., Severinghaus, J.P., Kawamura, K., Yoo, H.-S., Lee, J.B., Kim, J.S., 2006. A redetermination of the isotopic abundances of atmospheric Ar. Geochimica et Cosmochimica Acta 70, 4507–4512.

Lefebvre, C.J.C., Barnhoorn, A., van Hinsbergen, D.J.J., Kaymakcı, N., Vissers, R.L.M., 2011. Late Cretaceous extensional denudation along a marble detachment fault zone in the Kırşehir massif near Kaman, Central Turkey. Journal of Structural Geology 33, 1220–1236.

Lefebvre, C.J.C., Barnhoorn, A., van Hinsbergen, D.J.J., Kaymakcı, N., Vissers, R.L.M., 2012. Reply to Yurur and Genc's comment on Late Cretaceous extensional denudation along a marble detachment fault zone in the Kırşehir massif near Kaman, Central Turkey. Journal of Structural Geology 36, 90–93.

Lefebvre, C.J.C., Peters, K., Wehrens, P., Brouwer, F.M., van Hinsbergen, D.J.J., Kaymakcı, N., Vissers, R.L.M., van Roermund, H.L.M., Advokaat, E.L., Hendriks, B.W.H. and Corfu, F., submitted for publication. P-T-t-d evolution and extensional exhumation history of a "high-temperature complex" (Hırkadağ block, Central Anatolia). Lithos.

Luterbacher, H.P., Ali, J.R., Brinkhuis, H., Gradstein, F.M., Hooker, J.J., Monechi, S., Ogg, J.G., Powell, J., Röhl, U., Sanfilippo, A., Schmitz, B., 2004. The Paleogene period. In: Gradstein, F.M., Ogg, J.G., Smith, A.B. (Eds.), A Geological Timescale 2004. Cambridge University Press, Cambridge, pp. 384–408.

McDougall, I., Harrison, T.M., 1999. Geochronology and thermochronology by the ^{40}Ar/^{39}Ar method. Oxford University Press, New York.

McFadden, P.L., Lowes, F.J., 1981. The discrimination of mean directions drawn from Fisher distributions. Geophysical Journal of the Royal Astrological Society 67, 19–33.

McFadden, P.L., McElhinny, M.W., 1988. The combined analysis of remagnetisation circles and direct observations in paleomagnetism. Earth and Planetary Science Letters 87, 161–172.

McFadden, P.C., McElhinny, M.W., 1990. Classification of the reversal test in palaeomagnetism. Geophysical Journal International 103, 725–729.

Meijers, M.J.M., Kaymakcı, N., van Hinsbergen, D.J.J., Langereis, C.G., Stephenson, R.A., Hippolyte, J.-C., 2010a. Late Cretaceous to Paleocene oroclinal bending in the Central Pontides (Turkey). Tectonics 29, TC4016, http://dx.doi.org/10.1029/2009TC002620.

Meijers, M.J.M., Langereis, C.G., van Hinsbergen, D.J.J., Stephenson, R.A., Altiner, D., 2010b. Jurassic–Cretaceous low paleolatitudes from the circum-Black Sea region (Crimea and Pontides) due to true polar wander. Earth and Planetary Science Letters 296, 210–226.

Mullender, T.A.T., Van Velzen, A.J., Dekkers, M.J., 1993. Continuous drift correction and separate identification of ferrimagnetic and paramagnetic contribution in thermamagnetic runs. Geophysical Journal International 114, 663–672.

Okay, A.I., 1984. Distribution and characteristics of the northwest Turkish blueschists. In: Dixon, J.E., Robertson, A.H.F. (Eds.), The Geological Evolution of the Eastern Mediterranean: Geological Society, London, Special Publication, 17, pp. 455–466.

Okay, A.I., 1986. High pressure/low temperature metamorphic rocks of Turkey. In: Evans, B., Brown, E.H. (Eds.), Blueschists and Eclogites: Geological Society of America Memoir, 164, pp. 333–348.

Okay, A.I., 2008. Geology of Turkey: a synopsis. Anschnitt 21, 19–42.

Okay, A.I., Satir, M., Maluski, H., Siyako, M., Monié, P., Metzger, R., Akyüz, S., 1996. Paleo- and Neo-Tethyan events in northwestern Turkey: geologic and geochronologic constraints. In: Yin, A., Harrison, T.M. (Eds.), The Tectonic Evolution of Asia. Cambridge University Press, Cambridge, pp. 420–441.

Okay, A.I., Tansel, I., Tüysüz, O., 2001. Obduction, subduction and collision as reflected in the Upper Cretaceous–Lower Eocene sedimentary record of western Turkey. Geological Magazine 138, 117–142.

Okay, A.I., Tüysüz, O., Satir, M., Özkan-Altiner, S., Altiner, D., Sherlock, S., Eren, R.H., 2006. Cretaceous and Triassic subduction-accretion, high-pressure–low-temperature metamorphism, and continental growth in the Central Pontides, Turkey. Geological Society of America Bulletin 118, 1247–1269.

Pourteau, A., Candan, O., Oberhänsli, R., 2010. High-pressure metasediments in central Turkey: constraints on the Neotethyan closure history. Tectonics 29, TC5004, http://dx.doi.org/10.1029/2009TC002650.

Renne, P.R., Mundil, R., Balco, G., Min, K., Ludwig, K.R., 2010. Joint determination of ^{40}K decay constants and ^{40}Ar*/^{40}K for the Fish Canyon sanidine standard, and improved accuracy for ^{40}Ar/^{39}Ar geochronology. Geochimica et Cosmochimica Acta 74, 5349–5367.

Riba, O., 1976. Syn-tectonic unconformities of the Alto Cardener, Spanish Pyrenees: a genetic interpretation. Sedimentary Geology 15, 213–233.

Rice, S.P., Robertson, A.H.F., Ustaömer, T., 2006. Late Cretaceous–Early Cenozoic tectonic evolution of the Eurasian active margin in the Central and Eastern Pontides, northern Turkey. In: Robertson, A.H.F., Mountrakis, D. (Eds.), Tectonic Development of the Eastern Mediterranean Region. Geological Society, Special Publications, London, pp. 413–445.

Sanver, M., Ponat, E., 1981. Palaeomgnetic results from Kırşehir and surrounding area — rotation of the Kırşehir massif. Istanbul Yerbilimleri 2, 231–238.

Şengör, A.M.C., Yılmaz, Y., 1981. Tethyan evolution of Turkey: a plate tectonic approach. Tectonophysics 75, 181–241.

Şengör, A.M.C., Görür, N., Saroglu, F., 1985. Strike-slip faulting and related basin formation in zones of tectonic escape: Turkey as a case study. In: Biddle, K.T., Christie-Blick, N. (Eds.), Basin Formation and Sedimentation: Society of Economic Paleontologists and Mineralogists Special Publications, pp. 227–264.

Seymen, I., 1981. Stratigraphy and metamorphism of the Kırşehir Massif around Kaman (Kırşehir–Turkey). Bulletin of the Geological Society of Turkey 24, 7–14.

Tauxe, L., Kent, D.V., 2004. A simplified statistical model for the geomagnetic field and the detection of shallow bias in paleomagnetic inclinations: was the ancient magnetic field dipolar? In: Channell, J.E.T., Kent, D.V., Lowrie, W., Meert, J.G. (Eds.), Timescales of the Paleomagnetic field, Geophysical Monograph. American Geophysical Union, pp. 101–115.

Tauxe, L., Kodama, K.P., Kent, D.V., 2008. Testing corrections for paleomagnetic inclination error in sedimentary rocks: a comparative approach. Physics of the Earth and Planetary Interiors 169, 152–165.

Tekin, U.K., Göncüoglu, M.C., Turhan, N., 2002. First evidence of Late Carnian radiolarians from the İzmir–Ankara suture complex, central Sakarya, Turkey: implications for the opening age of the İzmir–Ankara branch of Neo-Tethys. Geobios 35, 127–135.

Tirel, C., Gautier, P., van Hinsbergen, D.J.J., Wortel, M.J.R., 2009. Sequential development of metamorphic core complexes: numerical simulations and comparison to the Cyclades, Greece. In: van Hinsbergen, D.J.J., Edwards, M.A., Govers, R. (Eds.), Collision and collapse at the Africa–Arabia–Eurasia Subduction Zone: Geological Society, London, Special Publication, pp. 257–292.

Torsvik, T.H., Cocks, L.R.M., 2009. The Lower Palaeozoic palaeogeographical evolution of the northeastern and eastern peri-Gondwanan margin from Turkey to New Zealand. In: Bassett, M.G. (Ed.), Early Palaeozoic Peri-Gondwana Terranes: New Insights from Tectonics and Biogeography: Geological Society, London, Special Publications, pp. 3–21.

Torsvik, T.H., Müller, R.D., Van der Voo, R., Steinberger, B., Gaina, C., 2008. Global plate motion frames: toward a unified model. Reviews of Geophysics 41, RG3004, http://dx.doi.org/10.1029/2007RG000227.

Tüysüz, O., Dellaloglu, A.A., Terzioglu, N., 1995. A magmatic belt within the Neo-Tethyan suture zone and its role in the tectonic evolution of northern Turkey. Tectonophysics 243, 173–191.

van Hinsbergen, D.J.J., 2010. A key extensional metamorphic complex reviewed and restored: the Menderes Massif of western Turkey. Earth-Science Reviews 102, 60–76.

Vissers, R.L.M., Platt, J.P., Van der Wal, D., 1995. Late orogenic extension of the Betic Cordillera and the Alboran Domain: a lithospheric view. Tectonics 14 (4), 786–803.

Watson, G.S., 1983. Large sample theory of the Langevin distribution. Journal of Statistical Planning and Inference 8, 245–256.

Whitney, D.L., Hamilton, M.A., 2004. Timing of high-grade metamorphism in central Turkey and the assembly of Anatolia. Journal of the Geological Society of London 161, 823–828.

Whitney, D.L., Teyssier, C., Dilek, Y., Fayon, A.K., 2001. Metamorphism of the Central Anatolian Crystalline Complex, Turkey: influence of orogen-normal collision vs wrench-dominated tectonics on P-T-t paths. Journal of Metamorphic Geology 19, 411–432.

Yalınız, K.M., Floyd, P.A., Göncüoglu, C.M., 2000a. Geochemistry of volcanic rocks from the Cicekdag Ophiolite, Central Anatolia, Turkey, and their inferred tectonic setting within the northern branch of the Neotethyan Ocean. In: Bozkurt, E., Winchester, J.A., Piper, J.D.A. (Eds.), Tectonics and magmatism in Turkey and the surrounding area: Geological Society, London, Special Publications, pp. 203–218.

Yalınız, K.M., Güncüoglu, M.C., Özkan-Altiner, S., 2000b. Formation and emplacement ages of the SSZ-type Neotethyan ophiolites in Central Anatolia, Turkey: palaeotectonic implications. Geological Journal 35, 53–68.

Yalınız, M.K., Floyd, P.A., Göncüoglu, M.C., 2000c. Petrology and geotectonic significance of plagiogranite from the Sarikaraman ophiolite (Central Anatolia, Turkey). Ofioliti 25, 31–37.

Yılmaz, S., Boztuğ, D., 1998. Petrogenesis of the Çiçekdag Igneous Complex, N of Kirsehir, Central Anatolia, Turkey. Turkish Journal of Earth Sciences 7, 185–199.

Yılmaz, A., Yılmaz, H., 2006. Characteristic features and structural evolution of a post collisional basin: the Sivas Basin, Central Anatolia, Turkey. Journal of Asian Earth Sciences 27, 164–176.

Yürür, M.T., Genç, Y., 2006. The Savcili thrust fault (Kirsehir region, central Anatolia): a backthrust fault, a suture zone or a secondary fracture in an extensional regime? Geological Carpathica 57, 47–56.

Zijderveld, J.D.A., 1967. A.C. demagnetisation of rocks: analysis of results. In: Collinson, D.W., et al. (Ed.), Methods in Palaeomagnetism. Elsevier, Amsterdam, pp. 254–286.